

Supporting Information

A novel multi-functional magnetic Fe-Ti-V spinel catalyst for elemental mercury capture and callback from flue gas

Shijian Yang,^a Yongfu Guo,^a Naiqiang Yan,^{a,*} Daqing Wu,^b Hongping He,^b Jiangkun Xie,^a Zan

Qu,^a Chen Yang^a and Jinping Jia^a

^a School of Environmental Science and Engineering, Shanghai Jiao Tong University, 800 Dong

Chuan Road, Shanghai, 200240 P. R. China

^b Guangzhou Institute of Geochemistry, Chinese Academy of Sciences, 511 Kehua Street, Wushan,

Tianhe District, Guangzhou, 510640 P. R. China

* Corresponding author phone: 86-21-54745591; e-mail: nqyan@sjtu.edu.cn (N.Q. Yan);

yangshijiangsq@163.com (S.J. Yang)

1. Experimental

1.1 Samples preparation

Nanosized $\text{Fe}_2\text{Ti}_{0.6}\text{V}_{0.4}\text{O}_4$ was prepared using a co-precipitation method. Suitable amounts of titanium tetrachloride, ferrous sulfate and vanadyl dichloride were dissolved in distilled water (cation concentration $\approx 0.3 \text{ mol L}^{-1}$). This mixture was added to an ammonium hydroxide solution, leading to an instantaneous precipitation. During the reaction, the system was continuously stirred at 800 rpm. The particles were then separated by centrifugation at 4500 rpm for 5 min and washed with distilled water followed by a new centrifugation. After 3 washings, the particles were collected and dried in a vacuum oven at 105 °C for 12 h. Non-stoichiometric Fe-Ti-V spinel ($\text{Fe}_2\text{Ti}_{0.6}\text{V}_{0.4}\text{O}_{4+\delta}$) was obtained after the thermal treatment of $\text{Fe}_2\text{Ti}_{0.6}\text{V}_{0.4}\text{O}_4$ under air at 400 °C for 3 h. Meanwhile, some cation vacancies (\square) were incorporated to compensate for the oxidization of V^{4+} and Fe^{2+} cations.

2.2 Samples characterization

Crystal structure of $\text{Fe}_2\text{Ti}_{0.6}\text{V}_{0.4}\text{O}_{4+\delta}$ was determined using an X-ray diffractionmeter (BRUKER-AXS) between 10° and 80° at a step of 7° min^{-1} operating at 35 KV and 30 mA using Cu K α radiation.

BET surface area was determined using a nitrogen adsorption apparatus (ASAP 2010 M+C, Micromeritics Inc.). All the samples were outgassed at 200 °C before BET measurements.

Saturation magnetization was determined using a vibrating sample magnetometer (VSM, Model JDM-13) at room temperature.

Transmission electron microscopy (TEM) was performed on a JEOL JEM-2010 TEM. The micrographs were obtained in the bright-field imaging mode at an acceleration voltage of 200 kV.

Temperature programmed desorption (TPD) was carried on a chemisorption analyzer (Micromeritics, AutoChem 2920). Before the experiment, about 0.15 g of sample was pretreated under He atmosphere at 400 °C for 60 min to remove the adsorbed H_2O and other gases. After the sample was cooled to 45 °C, the He flow was switched to a flow of 10% NH_3/He (15 ml min^{-1}) for 90 min. The sample was then purged by He (30 ml min^{-1}) for another 180 min. NH_3 -TPD was preformed at a heating rate of 5 °C min^{-1} to 400 °C under He atmosphere.

X-ray photoelectron spectroscopy (XPS, Thermo ESCALAB 250) was used to determine the

binding energies of Fe 2p, V 2p, Ti 2p, O 1s and Hg 4f with Al K α ($h\nu=1486.6$ eV) as the excitation source. The C 1s line at 284.6 eV was taken as a reference for the binding energy calibration.

2.3 Elemental mercury capture

The assembly used for elemental mercury capture consisted of an elemental mercury permeation tube, a packed-bed reactor, a cold vapor atomic absorption spectrometer (CVAAS) and an online data acquisition system (shown in Fig. S1). A flow of air passed through the permeation tube and yielded a stable concentration of elemental mercury. A temperature control device was employed to keep the reactor at desired temperatures. The gas containing elemental mercury first passed through the blank tube, and then entered the CVAAS to determine the baseline. When the concentration of elemental mercury had fluctuated within $\pm 10\%$ for more than 30 min, the gas was diverted to pass through the adsorbent bed for the test. An exact amount of catalyst was inserted in the middle of the column reactor and then packed with quartz wool to support the catalyst layer and avoid its loss. It was demonstrated that quartz wool has no ability for elemental mercury capture.

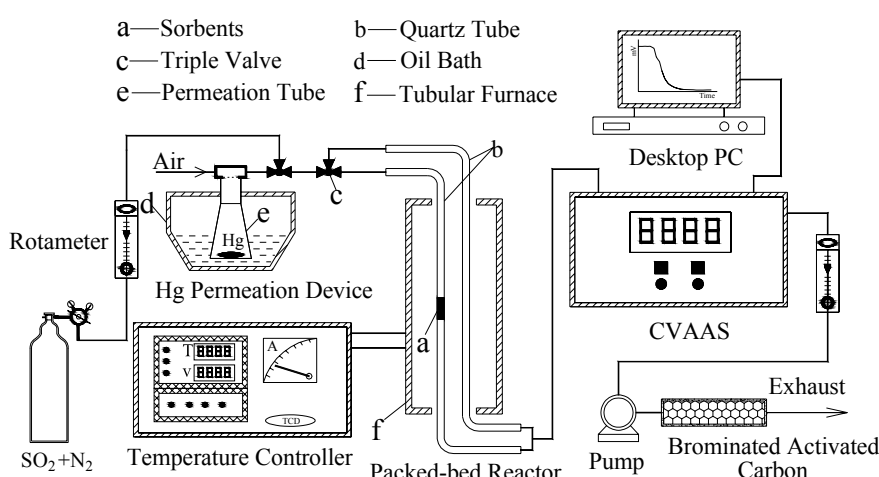


Fig. S1 Experimental system for packed-bed test

To estimate the performance for elemental mercury capture, $\text{Fe}_2\text{Ti}_{0.6}\text{V}_{0.4}\text{O}_{4+\delta}$ was first tested under air. The inlet gas contained about 0.60 mg Nm^{-3} ($\pm 10\%$) of elemental mercury with a feed of 12 L h^{-1} . For each test, the time was about 10 h, the catalyst mass was 300.0 mg (the gas space velocity was about $1.2 \times 10^5 \text{ h}^{-1}$) and the reaction temperature varied from 100–200 °C.

Then, the effect of a high concentration of SO₂ on elemental mercury capture by Fe₂Ti_{0.6}V_{0.4}O_{4+δ} was investigated. The simulated flue gas contained about 0.60 mg Nm⁻³ ($\pm 10\%$) of elemental mercury, 2.8 g Nm⁻³ (1000 ppm) of sulfur dioxide and 10% of O₂ with a feed of 12 L h⁻¹.

The catalytic decomposition of the formed mercury oxide by Fe₂Ti_{0.6}V_{0.4}O_{4+δ} was conducted at 100-300 °C. The inlet gas was air with a feed of 12 L h⁻¹.

The concentration of elemental mercury in the gas was analyzed using an SG-921 CVAAS. Meanwhile, the concentration of Hg²⁺ at the exit of reactor was determined using the Ontario Hydro Method.¹ Breakthrough curve was generated by plotting the CVAAS voltage signal.

2. Characterization results

2.1 XRD

Previous researches demonstrated that both vanadium and titanium can be incorporated into the structure of spinel using the co-precipitation method.²⁻⁵ The characteristic reflections of Fe₂Ti_{0.6}V_{0.4}O₄ (shown in Fig. S2a) corresponded very well to the standard card of magnetite (JCPDS: 19-0629). Additional reflections that would indicate the presence of other crystalline vanadium and titanium oxides, such as rutile, anatase, V₂O₅, VO₂, V₂O₄ or V₂O₃, were not present in the diffraction scan. It indicates that both V and Ti may be incorporated into the structure of spinel.²⁻⁵ After the thermal treatment at 400 °C for 3 h, a subtle reflection centered at 25.35° corresponding to anatase appeared in the XRD pattern of Fe₂Ti_{0.6}V_{0.4}O_{4+δ} (shown in Fig. S2b). It indicates that some Ti may be rejected from the spinel structure due to the compressive stresses in the spinel structure⁵ or some titanium was present in Fe₂Ti_{0.6}V_{0.4}O₄ as amorphous TiO₂, which may re-crystallize after the thermal treatment at 400 °C. Previous researches reported that the further oxidation of non-stoichiometric vanadium iron spinel was followed by a phase transition to α-Fe₂O₃, FeVO₄ and V₂O₅.^{3,6} In our previous research, it was demonstrated that the introduction of Ti had a stabilization effect on the spinel structure and the phase transition temperature shifted to a higher temperature with the increase of Ti content in (Fe_{3-x}Ti_x)_{1-δ}O₄.⁴ As a result, the reflections corresponding to α-Fe₂O₃, FeVO₄ and V₂O₅ were not present in the diffraction scan of

$\text{Fe}_2\text{Ti}_{0.6}\text{V}_{0.4}\text{O}_{4+\delta}$. After the 7 circulations, additional reflections corresponding to other crystalline oxides did not appear in Fig. S2c. It indicates that $\text{Fe}_2\text{Ti}_{0.6}\text{V}_{0.4}\text{O}_{4+\delta}$ was stable during the circulation.

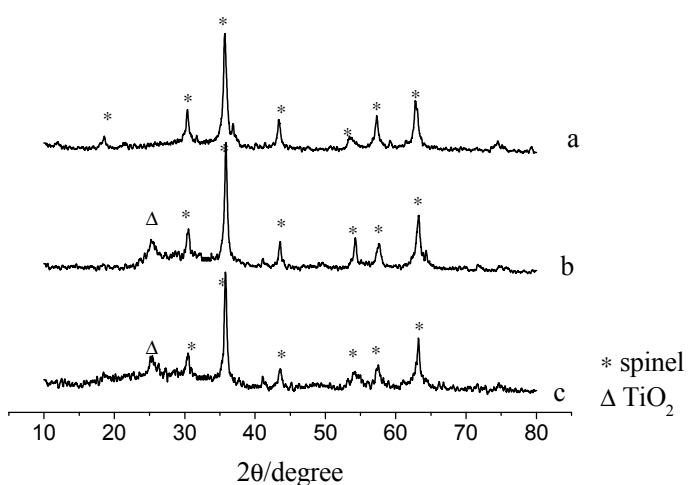


Fig. S2 XRD patterns of: (a), $\text{Fe}_2\text{Ti}_{0.6}\text{V}_{0.4}\text{O}_4$; (b), $\text{Fe}_2\text{Ti}_{0.6}\text{V}_{0.4}\text{O}_{4+\delta}$; (c), $\text{Fe}_2\text{Ti}_{0.6}\text{V}_{0.4}\text{O}_{4+\delta}$ after the 7 circulations.

2.2 TEM

TEM image (Fig. S3a) revealed irregular agglomerated nanoparticles of Fe-Ti-V oxide. The average particle size of $\text{Fe}_2\text{Ti}_{0.6}\text{V}_{0.4}\text{O}_{4+\delta}$ was about 20 nm. The EDX analysis showed that $\text{Fe}_2\text{Ti}_{0.6}\text{V}_{0.4}\text{O}_{4+\delta}$ mainly contained Fe, Ti, V and O, and other elements for example Cl and S were not detected (shown in Fig. S3b). Supplementary information was obtained from the selected area electron diffraction patterns (SAED). $\text{Fe}_2\text{Ti}_{0.6}\text{V}_{0.4}\text{O}_{4+\delta}$ showed obvious diffuse diffraction rings, as a consequence of the small crystallite sizes, that can be ascribed to the reflections of (200), (311), (400), (511) and (440) crystallographic planes of a cubic spinel phase.

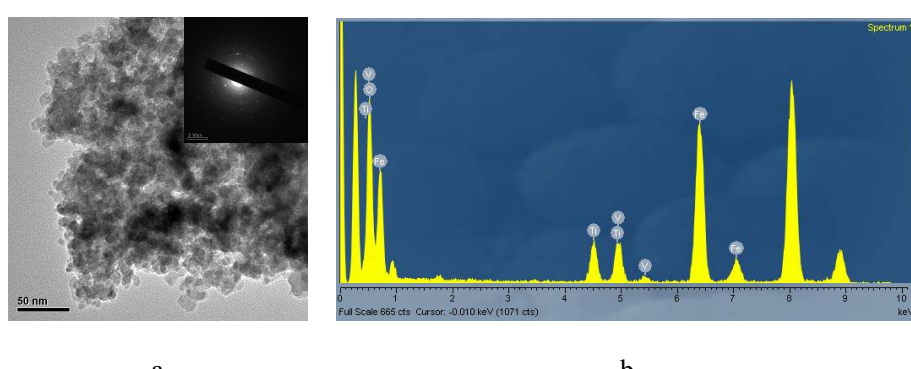


Fig. S3 (a), TEM image of $\text{Fe}_2\text{Ti}_{0.6}\text{V}_{0.4}\text{O}_{4+\delta}$; (b), EDX analysis of $\text{Fe}_2\text{Ti}_{0.6}\text{V}_{0.4}\text{O}_{4+\delta}$.

2.3 NH₃-TPD

Gaseous elemental mercury is a Lewis base because it can be an electron-pair donor. The term Lewis base is more general and refers to the propensity to complex with a Lewis acid. The Lewis acidity of Fe₂Ti_{0.6}V_{0.4}O_{4+δ} can be characterized by NH₃-TPD. NH₃-TPD analysis indicates that Fe₂Ti_{0.6}V_{0.4}O_{4+δ} had 6.5×10^{-3} mmol m⁻² of active sites on its surface. Fig. S4 shows the TPD profile of ammonia from Fe₂Ti_{0.6}V_{0.4}O_{4+δ}. Ammonia exhibited a maximum desorption rate at about 109 °C with a gradual tailing toward the higher temperature. 15%, 47%, 71%, 87% and 96% of adsorbed ammonia were desorbed from the surface at 100, 150, 200, 250 and 300 °C, respectively.

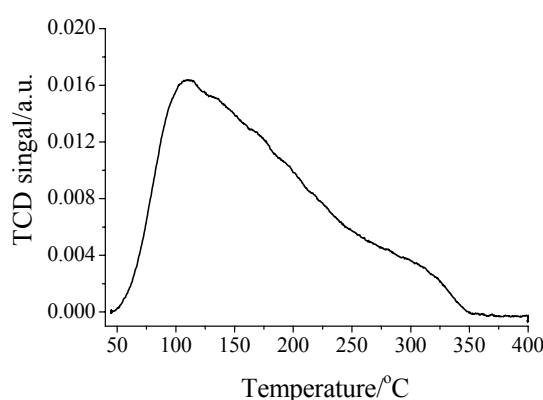


Fig. S4 NH₃-TPD profile of Fe₂Ti_{0.6}V_{0.4}O_{4+δ}.

2.4 XPS

Surface information of Fe₂Ti_{0.6}V_{0.4}O_{4+δ} was analyzed by XPS. XPS spectra over the spectral regions of Fe 2p, V 2p, Ti 2p and O 1s were evaluated (XPS spectra over the spectral region of V 2p are shown in Fig. S5).

The O 1s peaks mainly centered at about 530.2 eV, as expected for transition metal oxides. Another oxygen species centered at about 531.7 eV was also observed, which was assigned to hydroxyl group (-OH).⁷ The Ti peaks were assigned to Ti 2p 1/2 (464.4 eV) and Ti 2p 3/2 (458.7 eV) of Ti⁴⁺.

The Fe peaks were assigned to oxidized Fe species, more likely Fe³⁺ type species.⁷ The binding energies centered at about 710.4 and 711.3 eV may be assigned to Fe³⁺ cations in the spinel

structure, and the binding energy centered at about 712.7 eV was ascribed to Fe^{3+} bonded with hydroxyl groups ($\equiv \text{Fe}^{\text{III}} - \text{OH}$).

The V peaks were assigned to V^{5+} (517.4 eV) and V^{4+} (516.6 eV). XPS analysis showed that the ratios of V^{5+} to V^{4+} were about 1.27, 2.13 and 1.77 for $\text{Fe}_2\text{Ti}_{0.6}\text{V}_{0.4}\text{O}_{4+\delta}$, $\text{Fe}_2\text{Ti}_{0.6}\text{V}_{0.4}\text{O}_{4+\delta}$ after the adsorption at 100 °C and $\text{Fe}_2\text{Ti}_{0.6}\text{V}_{0.4}\text{O}_{4+\delta}$ after the desorption at 300 °C, respectively. It indicates that some V^{5+} cations may be reduced to V^{4+} cations to sustain the spinel structure with the increase of thermal treatment temperature.

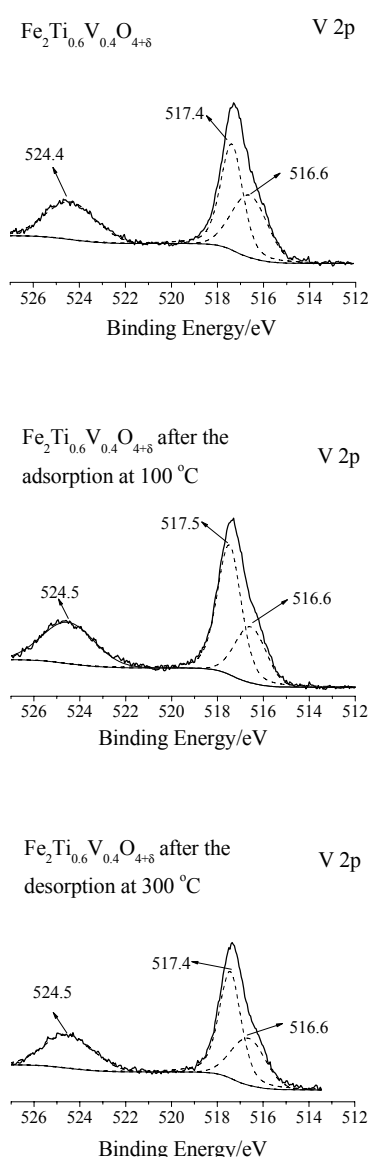


Fig. S5 XPS spectra of $\text{Fe}_2\text{Ti}_{0.6}\text{V}_{0.4}\text{O}_{4+\delta}$, $\text{Fe}_2\text{Ti}_{0.6}\text{V}_{0.4}\text{O}_{4+\delta}$ after the adsorption at 100 °C and $\text{Fe}_2\text{Ti}_{0.6}\text{V}_{0.4}\text{O}_{4+\delta}$ after the desorption at 300 °C over the spectral region of $\text{V} 2\text{p}$

3. Comparison of $\text{Fe}_2\text{Ti}_{0.6}\text{V}_{0.4}\text{O}_{4+\delta}$ with other sorbents

Table S1 compares the performance of $\text{Fe}_2\text{Ti}_{0.6}\text{V}_{0.4}\text{O}_{4+\delta}$ for elemental mercury capture with those of other sorbents.

Table S1 Comparison of the performance of $\text{Fe}_2\text{Ti}_{0.6}\text{V}_{0.4}\text{O}_{4+\delta}$ with other sorbents

Sorbent	Capacity /mg g ⁻¹	Carrier gas	Temperature /°C	magnetization /emu g ⁻¹	Regeneration Yes/No
I-AC ⁸	0.85	Air	140 °C	-	No
S-AC ⁹	1.9	Simulated fuel gas	140 °C	-	No
Cl-AC ¹⁰	4.0	Ar	138 °C	-	No
$\text{V}_2\text{O}_5/\text{TiO}_2$ ¹¹	0.23	Air	100 °C	-	No
$\text{MnO}_2/\text{Al}_2\text{O}_3$ ¹⁰	3.5	Air	138 °C	-	No
Z-Ag ⁰ ¹²	0.5	Ar	150 °C	-	Yes
Pd/ Al_2O_3 ¹³	0.9	Simulated fuel gas	288 °C	-	Yes
($\text{Fe}_2\text{Ti})_{1-\delta}\text{O}_4$	1.0 <0.2	Air with SO_2	250 °C 100 °C	28	No
($\text{Fe}_{2.2}\text{Mn}_{0.8})_{1-\delta}\text{O}_4$	1.9	Air with SO_2	150 °C	46	No
($\text{Fe}_2\text{Ti}_{0.5}\text{Mn}_{0.5})_{1-\delta}\text{O}_4$	4.2	Air with SO_2	150 °C	31	No
MagZ-Ag ⁰ ¹⁴	0.044	Ar	150 °C	40	Yes
$\text{Fe}_2\text{Ti}_{0.6}\text{V}_{0.4}\text{O}_{4+\delta}$	1.0	Air with SO_2	100 °C	26	Yes

Pretreated powdered activated carbon (I-AC, S-AC, Cl-AC) showed excellent capacities for elemental mercury capture. Direct injection of pretreated powdered activated carbon into the flue gas upstream of a particulate collector is currently considered the maximum available control technology for the removal of elemental mercury form the flue gas in coal-fired utilities, since almost all coal-fired power plants are equipped with an electrostatic precipitator or a baghouse.¹⁵ However, the separation of powdered activated carbon from the fly ash was extremely difficult and impractical. The fly ash with a large amount of activated carbon can not be directly used. Furthermore, the fly ash would be contaminated by the formed mercury dihalide.

SCR catalysts are mainly employed to reduce NO_x concentration in the flue gas, and elemental mercury may be removed as a cobenefit. The catalyst is typically composed of vanadium pentoxide (V_2O_5) supported on titanium dioxide (TiO_2). Laboratory-scale tests verify that SCR can oxidize Hg^0 to Hg^{2+} , particularly in the presence of HCl.^{11, 16} But in the absence of HCl, the

capacity of supported V₂O₅ for elemental mercury is very poor. Furthermore, the injection of ammonia for the necessary NO_x control is a severe interferent for elemental mercury capture.¹⁷

Development of metal and metal oxide sorbents can be used as an alternative.¹⁸ Some metals and metal oxides showed excellent capacities for elemental mercury capture (for example MnO₂/Al₂O₃, Z-Ag and Pd/Al₂O₃). Some of them can be thermal regenerated after elemental mercury capture. However, the separation of the sorbent from the fly ash was still difficult. The separation of the sorbent from the fly ash can be achieved by the magnetic property of sorbent material,¹⁴ so some magnetic nanoparticles (Fe_{3-x}Ti_x)_{1-δ}O₄, (Fe_{3-x}Mn_x)_{1-δ}O₄ and (Fe₂Ti_xMn_{1-x})_{1-δ}O₄ were developed as the sorbents for elemental mercury capture in our previous researches. Especially, (Fe₂Ti_{0.5}Mn_{0.5})_{1-δ}O₄ showed an excellent capacity for elemental mercury and the presence of a high concentration of SO₂ resulted in an insignificant effect. The decomposition temperature of HgO under air is about 500 °C. During the thermal treatment at 500 °C under air, the phase transition of (Fe₂Ti_{0.5}Mn_{0.5})_{1-δ}O₄ would happen and the magnetic property would disappear. A magnetic sorbent MagZ-Ag⁰ sorbent can be thermally regenerated at 400 °C.¹⁴ However, its capacity for elemental mercury capture was very small and its cost was expensive due to the use of noble metal Ag. Fe₂Ti_{0.6}V_{0.4}O_{4+δ} showed an excellent performance for elemental mercury capture in the presence of SO₂ at 100 °C. After being separated together with Fe₂Ti_{0.6}V_{0.4}O_{4+δ} from the fly ash using magnetic separation, the formed HgO can be catalytically decomposed at 300 °C to reclaim elemental mercury and regenerate the catalyst.

Notes and references

1. S. X. Wang, L. Zhang, G. H. Li, Y. Wu, J. M. Hao, N. Pirrone, F. Sprovieri and M. P. Ancora, *Atmos. Chem. Phys.*, 2010, **10**, 1183-1192.
2. V. Nivoix and B. Gillot, *Chem. Mater.*, 2000, **12**, 2971-2976; S. J. Yang, H. P. He, D. Q. Wu, D. Chen, Y. H. Ma, X. L. Li, J. X. Zhu and P. Yuan, *Ind. Eng. Chem. Res.*, 2009, **48**, 9915-9921.
3. V. Nivoix and B. Gillot, *Solid State Ion.*, 1998, **111**, 17-25; B. Gillot and V. Nivoix, *Mater. Res. Bull.*, 1999, **34**, 1735-1747.
4. S. Yang, H. He, D. Wu, D. Chen, X. Liang, Z. Qin, M. Fan, J. Zhu and P. Yuan, *Appl. Catal. B-environ.*, 2009, **89**, 527-535.
5. N. Guigue-Millot, Y. Champion, M. J. Hytch, F. Bernard, S. Begin-Colin and P. Perriat, *J. Phys. Chem. B*, 2001, **105**, 7125-7132.
6. V. Nivoix and B. Gillot, *Mater. Chem. Phys.*, 2000, **63**, 24-29.
7. T. Herranz, S. Rojas, M. Ojeda, F. J. Perez-Alonso, P. Tefferos, K. Pirota and J. L. G. Fierro, *Chem. Mater.*, 2006, **18**, 2364-2375; Y. Zhang, M. Yang, X. M. Dou, H. He and D. S. Wang, *Environ. Sci. Technol.*, 2005, **39**, 7246-7253.
8. S. F. Lee, Y. C. Seo, J. Jurng and T. G. Lee, *Atmos. Environ.*, 2004, **38**, 4887-4893.
9. H. C. Hsi, M. J. Rood, M. Rostam-Abadi, S. G. Chen and R. Chang, *Environ. Sci. Technol.*, 2001, **35**, 2785-2791.
10. E. J. Granite, H. W. Pennline and R. A. Hargis, *Ind. Eng. Chem. Res.*, 2000, **39**, 1020-1029.
11. W. J. Lee and G. N. Bae, *Environ. Sci. Technol.*, 2009, **43**, 1522-1527.
12. Y. Liu, D. J. A. Kelly, H. Q. Yang, C. C. H. Lin, S. M. Kuznicki and Z. G. Xu, *Environ. Sci. Technol.*, 2008, **42**, 6205-6210.
13. E. J. Granite, C. R. Myers, W. P. King, D. C. Stanko and H. W. Pennline, *Ind. Eng. Chem. Res.*, 2006, **45**, 4844-4848.
14. J. Dong, Z. H. Xu and S. M. Kuznicki, *Adv. Funct. Mater.*, 2009, **19**, 1268-1275; J. Dong, Z. H. Xu and S. M. Kuznicki, *Environ. Sci. Technol.*, 2009, **43**, 3266-3271.
15. Z. J. Mei, Z. M. Shen, Q. J. Zhao, W. H. Wang and Y. J. Zhang, *J. Hazard. Mater.*, 2008, **152**, 721-729; J. H. Pavlish, E. A. Sondreal, M. D. Mann, E. S. Olson, K. C. Galbreath, D. L. Laudal and S. A. Benson, *Fuel Process. Technol.*, 2003, **82**, 89-165.
16. Y. Li, P. D. Murphy, C. Y. Wu, K. W. Powers and J. C. J. Bonzongo, *Environ. Sci. Technol.*, 2008, **42**, 5304-5309.
17. C. W. Lee, S. D. Serre, Y. Zhao and S. J. Lee, *J. Air. Waste. Manage.*, 2008, **58**, 484-493; J. R. Strege, C. J. Zygarlicke, B. C. Folckedahl and D. P. McCollor, *Fuel*, 2008, **87**, 1341-1347; K. Schofield, *Environ. Sci. Technol.*, 2008, **42**, 9014-9030.
18. Z. J. Mei, Z. M. Shen, W. H. Wang and Y. J. Zhang, *Environ. Sci. Technol.*, 2008, **42**, 590-595.